PERGAMON

International Journal of Solids and Structures 38 (2001) 5765–5787

INTERNATIONAL JOURNAL OF SOLIDS and STRUCTURES

www.elsevier.com/locate/ijsolstr

Study on generation of rock fracture surfaces by using fractal interpolation ☆

Heping Xie *, Hongquan Sun, Yang Ju, Zhigang Feng

Institute of Rock Mechanics and Fractals, China University of Mining and Technology, D11, Xueyuan Road, Beijing 100083, People's Republic of China

Received 20 October 1999; in revised form 15 October 2000

Abstract

The mathematical model of a fractal interpolation surface on a rectangular field is proposed in this paper. The theory of a fractal interpolation surface is applied to the generation of rock fracture surfaces. The methods of the improved self-affine fractal interpolation surface are proposed. Based on the statistical fractal character of fracture surfaces, the new ideas and methods of the partition of the local field and the determination of a vertical scaling factor are given by using the principles of geostatistics and trend surface analyses, so that the local stochastic irregular roughness on the fracture surface can be simulated. Fractal interpolated surfaces based on 5.5–25.62% of information data on 12 measured rock fracture surfaces are in good agreement with the measured rock fracture surfaces, and the relationship of the information point number used in the interpolation and the interpolation precision is obtained.

Keywords: Fractal geometry; Fractal interpolation surface; Rock fracture surface; Surface roughness

1. Introduction

The earth's crust is basically discontinuous. The faults and joints in rocks affect the deformation, strength, and conductivity of rock masses significantly. Slope slides and roof caving occur too frequently in civil engineering and mining projects. The occurrences of accidents are closely related to the influence of faults and joints in rocks. Extensive investigations have shown that surface roughness of rock fracture plays an important role in the influence of the mechanical behavior of faults and rock joints (Barton, 1973; Byerlee, 1978; Bandis, 1990; Aydan and Kawamoto, 1990; Maerz and Franklin, 1990; Huang et al., 1992; Xie, 1993; Xie and Pariseau, 1994; Xie et al., 1998).

Fractal geometry established on the pioneering work of Mandelbrot (1982a,b) has attracted a great amount of interest and attention from scientists in recent years. Fractal theory quantitatively describes an

☆ Supported by China National Nature Science Funds (ratified no. 50074032 and 19702021) and China National Distinguished Youth's Science Funds (ratified no. 59425003).

* Corresponding author. Tel.: +86-10-6233-1286/1358; fax: +86-10-6232-5016.
E-mail address: xieph@mail.cumtb.edu.cn (H. Xie).

0020-7683/01/$ - see front matter
PII: S0020-7683(00)00390-5

irregular (fractal) object. The feature of fractal geometry can be expressed mathematically with self-similarity and self-affinity, suggesting that the structural phenomena exist at any scale. Some pioneer investigations have used fractal geometry as an alternate tool to characterize the rough surfaces of rock joints (Turk et al., 1987; Xie, 1989; Maerz and Franklin, 1990; Lee et al., 1990; Huang et al., 1992; Muralha, 1992; Odling, 1994; Xie, 1993; Xie and Sanderson, 1994, 1995; Xie et al., 1997). From these works, it has been discovered that the rough surfaces of rock joints have some fractal features and the fractal dimension is one of the surface morphology parameters of the discontinuities.

So far, many of the studies have been limited in descriptions of the rough surfaces of rock fractures. The most important aspect in rock engineering practice, however, is that fractal analysis may be applied to predict the mechanical properties and behavior of rock engineering situations, especially when faults and joints are in different strata where it is impossible to obtain the detailed data on the roughness of the fault surfaces directly. It is urgent and invaluable to setup mathematical models of fractals (Xie and Sun, 1997) so that the real fault morphology can be interpolated approximately based on limited amount of measured data of surface roughness. The work described herein includes two parts: (1) the method of an improved self-affine fractal interpolation surface is put forward based on the fractal interpolation surfaces described in the literature (Manderbrot, 1982a,b; Barnsley and Pemko, 1986; Feder, 1988; Massopust, 1994), (2) a comparison of mathematically generated morphology of rock fracture surfaces with measured parameters. The study emphasizes the precision of fractal interpolation of rock fracture surfaces. In order to simulate local stochastic irregular roughness of the natural fracture surfaces, the new ideas and methods of the partition of the local field and determination of a vertical scaling factor are given by using the principles of geostatistics and trend surface analysis. To confirm results of the fractal interpolation method, the roughness data of the fracture surfaces of 12 rock samples measured by using a laser scanner in the laboratory are used to carry out the fractal interpolation of fracture surfaces. With the method discussed in this paper, the descriptions of the surfaces with higher interpolation precision are obtained.

2. The establishment of fractal interpolation surfaces on a rectangle field

Let $I = [a, b]$, $J = [c, d]$; and $D = I \times J = \{(x, y) : a \leqslant x \leqslant b, c \leqslant y \leqslant d\}$. We divide D into grids with the steps Δx and Δy such that (Qi, 1994)

$$\begin{cases} a = x_0 < x_1 < \cdots < x_N = b \\ c = y_0 < y_1 < \cdots < y_M = d \end{cases} \tag{1}$$

With a data set $\{(x_i, y_j, z_{i,j}),\ i = 0, 1, \ldots, N,\ j = 0, 1, \ldots, M\}$ on the grids, we construct an interpolation function $f : D \to R$, such that $f(x_i, y_j) = z_{i,j}$, $i = 0, 1, \ldots, N$, $j = 0, 1, \ldots, M$.

We will restrict our attention to the field $K = D \times [h_1, h_2] (-\infty < h_1 < h_2 < +\infty =$. For (c_1, d_1, e_1), $(c_2, d_2, e_2) \in K$, let $d((c_1, d_1, e_1), (c_2, d_2, e_2)) = \max\{|c_1 - c_2|, |d_1 - d_2|, |e_1 - e_2|\}$.

2.1. Iteration function system

Let $I_n = [x_{n-1}, x_n]$, $J_m = [y_{m-1}, y_m]$, $D_{n,m} = I_n \times J_m$, $n \in \{1, 2, \ldots, N\}$, $m \in \{1, 2, \ldots, M\}$. And let $\Phi_n : I \to I_n$, $\Psi_m : J \to J_m$ be contraction mapping, so that:

$$\begin{cases} \Phi_n(x_0) = x_{n-1}, \qquad \Phi_n(x_N) = x_n \\ \Psi_m(y_0) = y_{m-1}, \qquad \Psi_m(y_M) = y_m \\ |\Phi_n(c_1) - \Phi_n(c_2)| < k_1 |c_1 - c_2| \\ |\Psi_m(d_1) - \Psi_m(d_2)| < k_2 |d_1 - d_2| \end{cases} \tag{2}$$

where $c_1, c_2 \in I$, $d_1, d_2 \in J$, $0 \leqslant k_1 < 1$, $0 \leqslant k_2 < 1$.

Let $L_{n,m}: D \to R^2$ be a contraction transformation: $L_{n,m}(x,y) = (\Phi_n(x), \Psi_m(y))$. Let $F_{n,m}: K \to [h_1, h_2]$ be continuous, which must obey four equations:

$$\begin{cases} F_{n,m}(x_0, y_0, z_{0,0}) = z_{n-1,m-1} \\ F_{n,m}(x_N, y_0, z_{N,0}) = z_{n,m-1} \\ F_{n,m}(x_0, y_M, z_{0,M}) = z_{n-1,m} \\ F_{n,m}(x_N, y_M, z_{N,M}) = z_{n,m} \end{cases} \tag{3}$$

For any $(c,d) \in D$ and $z_1, z_2 \in [h_1, h_2]$, we have

$$|F_{n,m}(c,d,z_1) - F_{n,m}(c,d,z_2)| \leqslant k_3 |z_1 - z_2| \quad n \in \{1,2,\ldots,N\}, \ \ m \in \{1,2,\ldots,M\}, \ \ 0 \leqslant k_3 < 1. \tag{4}$$

Let $\Phi_n(x) = a_n x + b_n$. With the condition (2), we have

$$a_n x_0 + b_n = x_{n-1}, \quad a_n x_N + b_n = x_n,$$

and obtain

$$\begin{cases} a_n = (x_n - x_{n-1})/(x_N - x_0) \\ b_n = (x_{n-1} x_N - x_n x_0)/(x_N - x_0) \end{cases} \tag{5}$$

$$\therefore \ \Phi_n(x) = x_{n-1} + \frac{x_n - x_{n-1}}{x_N - x_0}(x - x_0) \quad n \in \{1,2,\ldots,N\} \tag{6}$$

Let $\Psi_m(y) = c_m y + d_m$. Similarly, with the condition (2), we have

$$\begin{cases} c_m = (y_m - y_{m-1})/(y_M - y_0) \\ d_m = (y_{m-1} y_M - y_m y_0)/(y_M - y_0) \end{cases} \tag{7}$$

$$\therefore \ \Psi_m(y) = y_{m-1} + \frac{y_m - y_{m-1}}{y_M - y_0}(y - y_0) \quad m \in \{1,2,\ldots,M\} \tag{8}$$

Let

$$F_{n,m}(x,y,z) = e_{n,m} x + f_{n,m} y + g_{n,m} xy + s_{n,m} z + k_{n,m} \quad n \in \{1,2,\ldots,N\}, \ \ m \in \{1,2,\ldots,M\} \tag{9}$$

According to Eq. (3), we have

$$\begin{cases} z_{n-1,m-1} = e_{n,m} x_0 + f_{n,m} y_0 + g_{n,m} x_0 y_0 + s_{n,m} z_{0,0} + k_{n,m} \\ z_{n,m-1} = e_{n,m} x_N + f_{n,m} y_0 + g_{n,m} x_N y_0 + s_{n,m} z_{N,0} + k_{n,m} \\ z_{n-1,m} = e_{n,m} x_0 + f_{n,m} y_M + g_{n,m} x_0 y_M + s_{n,m} z_{0,M} + k_{n,m} \\ z_{n,m} = e_{n,m} x_N + f_{n,m} y_M + g_{n,m} x_N y_M + s_{n,m} z_{N,M} + k_{n,m} \end{cases} \tag{10}$$

Let $s_{n,m}$ $(n \in \{1,2,\ldots,N\}, m \in \{1,2,\ldots,M\})$ be any real number and satisfy $|s_{n,m}| < 1$ that is called a vertical scaling factor. We find that we can always solve the above equations for $e_{n,m}$, $f_{n,m}$, $g_{n,m}$ and $k_{n,m}$ in terms of the interpolation data and $s_{n,m}$. We obtain

$$\begin{cases} g_{n,m} = \frac{z_{n-1,m-1} - z_{n-1,m} - z_{n,m-1} + z_{n,m} - s_{n,m}(z_{0,0} - z_{N,0} - z_{0,M} + z_{N,M})}{x_0 y_0 - x_N y_0 - x_0 y_M + x_N y_M} \\ e_{n,m} = \frac{z_{n-1,m-1} - z_{n,m-1} - s_{n,m}(z_{0,0} - z_{N,0}) - g_{n,m}(x_0 y_0 - x_N y_0)}{x_0 - x_N} \\ f_{n,m} = \frac{z_{n-1,m-1} - z_{n-1,m} - s_{n,m}(z_{0,0} - z_{0,M}) - g_{n,m}(x_0 y_0 - x_0 y_M)}{y_0 - y_M} \\ k_{n,m} = z_{n,m} - e_{n,m} x_N - f_{n,m} y_M - s_{n,m} z_{N,M} - g_{n,m} x_N y_M \\ n \in \{1,2,\ldots,N\}, \ \ m \in \{1,2,\ldots,M\} \end{cases} \tag{11}$$

We define a new mapping $G_{n,m}(x,y,z)$:

$$G_{n,m}(x,y,z)=\begin{cases} F_{n,m}(x,y,z)+\Delta_{n,m}(y,z)\frac{x-x_{N-1}}{x_N-x_{N-1},} & x\in[x_{N-1},x_N],\ n\in\{1,2,\ldots,N-1\},\ m\in\{1,2,\ldots,M\},\\ F_{n+1,m}(x,y,z)-\Delta_{n,m}(y,z)\frac{x_1-x}{x_1-x_0}, & x\in[x_0,x_1],\ n\in\{1,2,\ldots,N-1\},\ m\in\{1,2,\ldots,M\},\\ F_{n,m}(x,y,z)+\Theta_{n,m}(x,z)\frac{y-y_{M-1}}{y_M-y_{M-1}}, & y\in[y_{M-1},y_M],\ n\in\{1,2,\ldots,N\},\ m\in\{1,2,\ldots,M-1\},\\ F_{n,m+1}(x,y,z)-\Theta_{n,m}(x,z)\frac{y_1-y}{y_1-y_0}, & y\in[y_0,y_1],\ n\in\{1,2,\ldots,N\},\ m\in\{1,2,\ldots,M-1\},\\ F_{n,m}(x,y,z), & \text{others,}\end{cases} \tag{12}$$

where

$$\Delta_{n,m}(y,z)=(F_{n+1,m}(x_0,y,z)-F_{n,m}(x_N,y,z))/2 \tag{13}$$

$$\Theta_{n,m}(x,z)=(F_{n,m+1}(x,y_0,z)-F_{n,m}(x,y_M,z))/2 \tag{14}$$

Eq. (12) can be described as follows (for the sake of simplification we only explain $F_{n,m}$ and $F_{n+1,m}$ on X direction). See Fig. 1. Generally, the interpolation results of $F_{n,m}$ and $F_{n+1,m}$ on common borderline are different if the boundary of the field is noncoplanar. In other words, the interpolation values are not unique. We construct the new mapping $G_{n,m}$ to remedy this shortcoming (see Fig. 2).

According to the Eq. (12), we can define an iterate function system (IFS) (Barnsley and Pemko, 1986; Barnsley, 1988) $W_{n,m}(x,y,z)$ on the field K:

$$W_{n,m}(x,y,z)=(\Phi_n(x),\Psi_m(y),G_{n,m}(x,y,z))\quad n\in\{1,2,\ldots,N\},\ m\in\{1,2,\ldots,M\}. \tag{15}$$

For such defined IFS, we have a unique attractor $G=\{(x,y,f(x,y)):(x,y)\in D\}$ that is the graph of a continuous function f, such that

$$f(x_i,y_j)=z_{i,j};\quad i=0,1,\ldots,N,\ \ j=0,1,\ldots,M \tag{16}$$

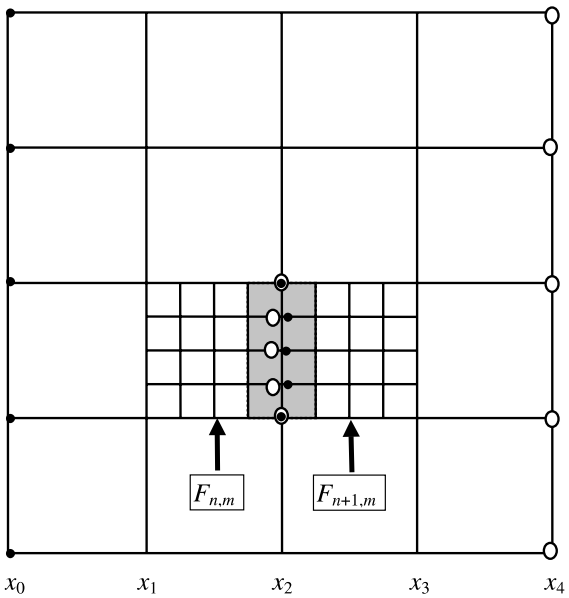

Fig. 1. The interpolation with noncoplanar boundary data: (•) – interpolation point on the left boundary, (○) – interpolation point on the right boundary, (□) – the area on the common boundary calculated by $F_{n,m}$ and $F_{n+1,m}$,⊙ – the point with the unique result interpolated by $F_{n,m}$ and $F_{n+1,m}$, (○•) – the point with the nonunique result interpolated by $F_{n,m}$ and $F_{n+1,m}$.

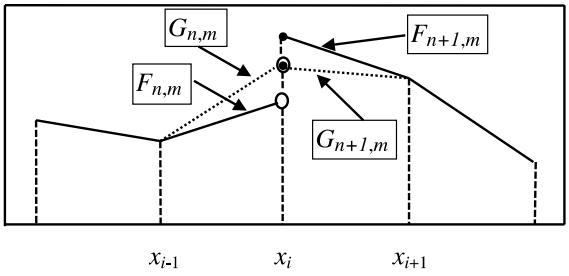

Fig. 2. The interpolated result of $G_{n,m}$ and $F_{n,m}$.

2.2. Interpolation function

Based on the IFS equation (15), the function of the self-affine fractal interpolation surface must satisfy:

$$f(x,y) = e_{n,m}\Phi_n^{-1}(x) + f_{n,m}\Psi_m^{-1}(y) + g_{n,m}\Phi_n^{-1}(x)\Psi_m^{-1}(y) + s_{n,m}f\left(\Phi_n^{-1}(x), \Psi_m^{-1}(y)\right) + k_{n,m} \tag{17}$$

where $e_{n,m}$, $f_{n,m}$, $g_{n,m}$ and $k_{n,m}$ are obtained from Eq. (11) and

$$\Phi_n^{-1}(x) = (x - x_{n-1})\frac{x_N - x_0}{x_n - x_{n-1}} + x_0, \quad x \in [x_{n-1}, x_n], \ \ n \in \{1, 2, \ldots, N\}, \tag{18}$$

$$\Psi_m^{-1}(y) = (y - y_{m-1})\frac{y_M - y_0}{y_m - y_{m-1}} + y_0, \quad y \in [y_{m-1}, y_m], \ \ m \in \{1, 2, \ldots, M\}. \tag{19}$$

2.3. Dimension of fractal interpolation surface

Let $N = M$ in Eq. (17) and $a_n = c_m = 1/N$ in Eqs. (5) and (7). So that

$$\begin{cases} \Phi_n = \frac{1}{N}x + b_n, & n \in \{1, 2, \ldots, N\} \\ \Psi_m = \frac{1}{N}y + d_m, & m \in \{1, 2, \ldots, N\} \end{cases} \tag{20}$$

The number of the fields for the interpolation is N^2 $(= N \times N)$. Let f^* denote the fractal interpolation function, the domain of f^* is $[a,b] \times [c,d]$. Then the graph of the function f^* (graph f^*) is a fractal surface in three-dimension Euclidean space R^3 on which the data (x_i, y_j, z_{ij}), $i, j = 0, 1, 2, \ldots, N$ lie. According to Massopust's research on fractal surface dimension (Massopust, 1994), we have the dimension theorem of a fractal interpolation function as follows:

Theorem. *Suppose* $\sum_{n=1}^{N}\sum_{m=1}^{N}|s_{n,m}| > N$ *and the interpolation points are noncoplanar, then the box dimension of fractal interpolation surface is given by*

$$\dim(\text{graph } f^*) = 1 + \log_N \sum_{n=1}^{N}\sum_{m=1}^{N}|s_{n,m}| \tag{21}$$

3. The case of a self-affine fractal interpolation surface

We get 10×10 data points measured on a rock fracture surface (Wang, 1994) (Table 1). With the self-affine fractal interpolation surface function, we will use these data to simulate the real rock fracture surface.

Table 1
The value of experimental variagram

h (cm)	Data pair	$\gamma^*(h)$
0.22	90	0.13
0.44	40	0.22
0.66	30	0.30
0.88	20	0.56
1.10	10	0.55

Fig. 3 shows the space distribution of these data and Fig. 4 gives an example of the fractal interpolated result (vertical scaling $s_{n,m} = 0.11$ and $\Delta x = \Delta y = 0.22$ cm).

Fig. 5 shows the rock fracture surface measured by a laser scanner. In Fig. 4, it can be easily found that the interpolated surface has higher symmetry and regularity because the strict self-affine fractal interpolation is used. This interpolated result indicates the fractal characteristics of strict self-affinity on mathe-

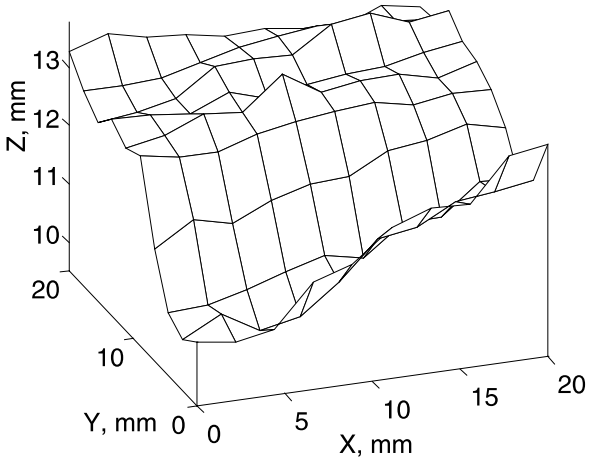

Fig. 3. The space distribution of 10×10 data measured from a rock fracture surface.

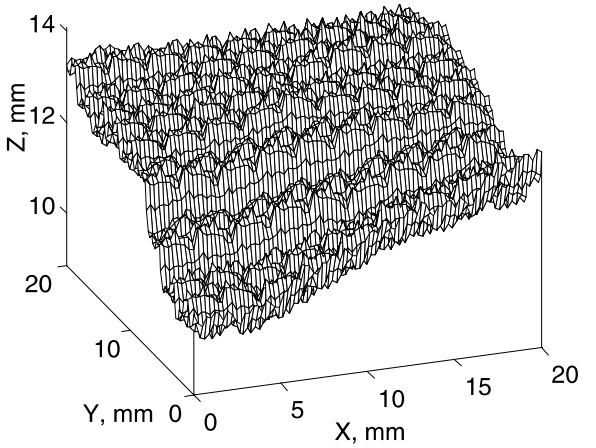

Fig. 4. The self-affine fractal interpolation surface (the vertical scaling $s_{n,m} = 0.11$).

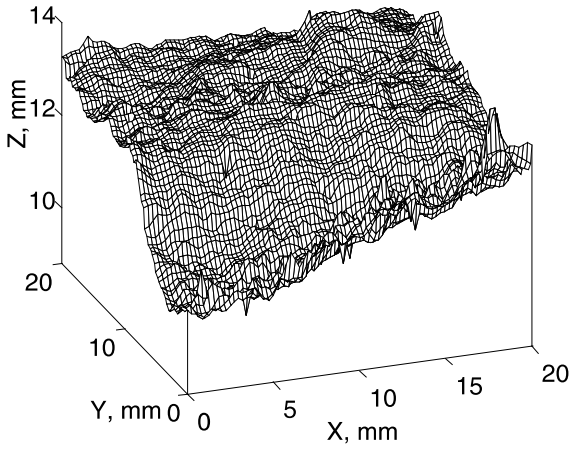

Fig. 5. Rock fracture surface measured by laser scanner (Wang, 1994).

matical theory. Unfortunately, natural rock fracture surface has fractal feature, but not strict self-affinity. Comparing Figs. 4 and 5, we can see that the morphology of this kind of interpolated surface is not consistent with the actual measured surface. So we put forward an improved self-affine fractal interpolation and setup the methods of the partition of local field and the determination of vertical scaling in this paper. With this method, we can obtain higher precision for the description of a fractal interpolation surface of a rock fracture surface.

4. Improved self-affine fractal interpolation

There is no strict self-affine fracture surface in nature. What we wish to do is to model the fracture surfaces by the self-affine fractal interpolation surfaces. How to interpolate a fracture surface with high precision and to satisfy the practical demand of engineering problems under restraints of a limited amount data is an application of wide general interest. In this section, a method of improved self-affine fractal interpolation is proposed. The goal of this improved self-affine fractal interpolation is to enhance interpolation precision based on the methods of the partition of the local field and determination of the vertical scaling.

4.1. Partition of the local field

According to the characteristics of local pertinence of rock fracture surfaces and the variagram theory in geostatistics (Sun, 1990), we put forward the method of local field partition to obtain higher interpolating precision. Let us first briefly introduce the principles of the variagram.

The variagram is a powerful research tool both pertinence and randomness. The model of a theoretical variagram reflects both the pertinence and the randomness of regional variables. The theoretical equation of the spherical variagram model is (see Fig. 6):

$$\gamma(h) = \begin{cases} c_0, & h = 0, \\ c_0 + c\left(\frac{3}{2}\frac{h}{a} - \frac{1}{2}\left(\frac{h}{a}\right)^3\right), & 0 < h \leqslant a, \\ c_0 + c, & h > a, \end{cases} \tag{22}$$

where a is range, c_0 nugget effect and $c_0 + c$ sill.

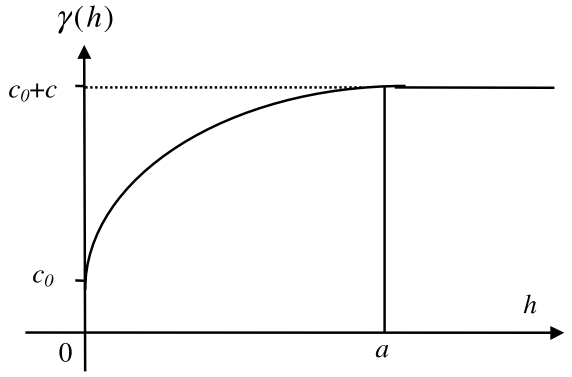

Fig. 6. Spherical variagram model.

Fig. 6 gives a spherical variagram model. The abscissa (h) stands for the distance between two points and the ordinate $(\gamma(h))$ the value of variagram (the magnitude of variability). From Fig. 6, we can see that the variability increases along a cubic curve when the distance, less than a, increases. When the distance between two points is greater than a, the variability stays on the value $c_0 + cc_0 + c$ is called the sill. It reflects the extent of data variation. The term c_0 denotes the nugget that expresses the discontinuity of data at the origin. It means that the variation produces the jump c_0 when the distance between two points is very small. The physical meaning of the range a can be explained as follows.

The variability of the two points is related to the distance between them if the distance is less than a (the larger the distance, the larger the variability). The variation of the curve on the interval $[0, a]$ reflects the pertinence of the data. When the distance of the two points is greater than a, the variability of the two points is independent of the distance between them. The variation of the curve on the interval (a, ∞) reflects the randomicity of the data. So we call a the range that is the extension of data variance. We can use the range a as the reference of the partition of the local field.

To obtain the theoretical variagram, we should make an experimental variagram first. The formula of the experimental variagram is

$$\gamma^*(h) = \frac{1}{2N(h)} \sum_{i=1}^{N(h)} [z(x_i + h) - z(x_i)]^2 \tag{23}$$

where $\gamma^*(h)$ is the experimental variagram, $z(x)$ is the altitude at x on the fracture surface, h is called lag that is the distance between two points and $N(h)$ is the total number of the data pairs.

We take data in Table 1 as a studying case. The experimental variagram is calculated with the lag (h) 0.22, 0.44, 0.66, 0.88 and 1.10 cm and listed in Table 2.

On the coordinate system $h - \gamma(h)$ the points are drawn in Fig. 7. Based on these points we use the least square method to fit a theoretical variagram curve Eq. (22) (see Fig. 7). Then we can obtain all the parameters of the theoretical variagram. The range a (one of the parameters of the theoretical variagram) is approximately equal to 0.7 cm. Thus based on the previous consideration we take 0.7 cm as the side of the local field.

According the value of range a, the interval of the interpolating points is determined to be 0.22 cm, so we use 4×4 interpolating points (3×3 intervals) as a local field (see Fig. 8). We will perform the interpolation on the local field, not the whole area.

Table 2
The relationship between fractal dimension and the number of information points

Surface type	Number of data	Information content (%)	The rock sample code												Average
			1	2	3	4	5	6	7	8	9	10	11	12	
Fractal interpolation surface	6×6	0.55	2.0309	2.0322	2.0289	2.0147	2.0335	2.0448	2.0399	2.0329	2.0278	2.0323	2.0301	2.0353	2.0319
	11×11	1.84	2.0379	2.0325	2.0395	2.0348	2.0324	2.0542	2.0576	2.0384	2.0094	2.0582	2.0361	2.0489	2.0400
	21×21	6.72	2.0469	2.0460	2.0549	2.0418	2.0412	2.0683	2.0717	2.0513	2.0192	2.0848	2.0468	2.0602	2.0528
	41×41	25.62	2.0528	2.0486	2.0575	2.0492	2.0465	2.0761	2.0792	2.0566	2.0213	2.0914	2.0538	2.0673	2.0584
Fracture surface	81×81	100	2.0679	2.0549	2.0685	2.0565	2.0575	2.0963	2.1038	2.0706	2.0406	2.1247	2.0646	2.0831	2.0741

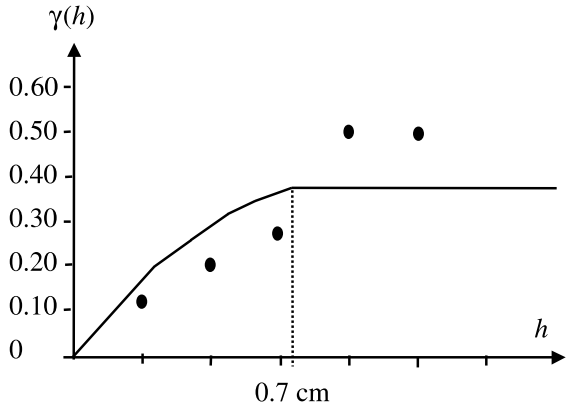

Fig. 7. The curve of fitting experimental variagram: (•) – data point of experimental variagram, (—) – curve of theoretical variagram, $a = 0.7$, $c_0 = 0$, $c_0 + c = 0.35$.

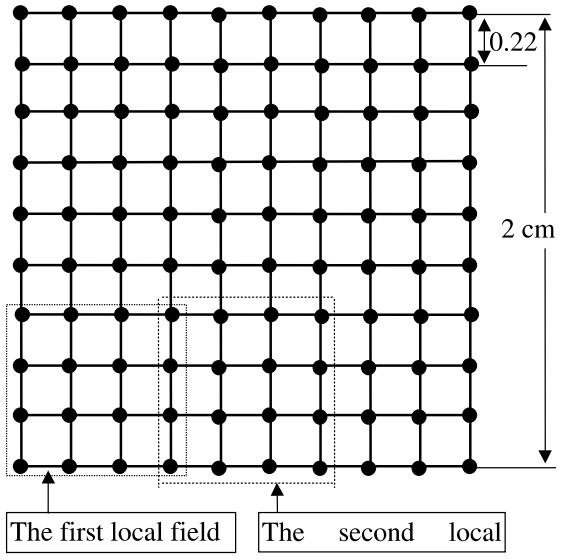

Fig. 8. The determination of local field.

4.2. The selection of the vertical scaling

From the fractal interpolation surface equation (17), we know that the parameters $g_{n,m}$, $e_{n,m}$, $f_{n,m}$ and $k_{n,m}$ can be found by using Eq. (11) and only $s_{n,m}$, vertical scaling, is a free parameter that influences the morphology of interpolated surfaces. Under the same interpolation conditions (interpolation model and interpolating data), different vertical scaling produces different interpolated surfaces.

In the present literature of fractal interpolation, the vertical scaling is given artificially. So the interpolated results can only satisfy the demand of theoretical research; they cannot meet the demand of practical engineering.

We discuss now the method of determining the vertical scaling that relates to the given interpolating data. So that we can obtain a high-precision interpolated fracture surface.

It is well known that the inhomogeneity of a material dominates the roughness of fracture surfaces. The interpolating data are taken from the fracture surface, so they express the degree of roughness of the fracture surface. On the other hand, the vertical scaling in the interpolation influences the roughness of the interpolated surface directly. Therefore, the selection of the vertical scaling should be based on the interpolated data. The methods and the process of determining the vertical scaling are as follows:

1. Based on the given data (interpolated data) (x_i, y_i, z_i) $(i = 1, 2, \ldots, n)$, use the least square method to fit one order trend surface equation: $z = b_0 + b_1 x + b_2 y$.
2. Using the one order trend surface equation, calculate the trend value at each given data point: $\hat{z}_i = b_0 + b_1 x_i + b_2 y_i$ $(i = 1, 2, \ldots, n)$.
3. Obtain the deviation value by subtracting the trend value from the corresponding given data: $e_i = z_i - \hat{z}_i$ $(i = 1, 2, \ldots, n)$.
4. Use the deviation value as the reference for the vertical scaling.

The one order trend surface expresses the average variational plane. The magnitude of the deviation value reflects the extent of departure for the given data from the average plane.

From the variagram principles, the data are pertinent within the area of the range a. In the small neighborhood of a given point, the variational feature at the point reflects that in the small neighborhood. So, using the deviation value at the point to estimate the vertical scaling in the neighborhood including the point is an unbiased estimation.

The equation of one order trend surface (Wang, 1982) can be expressed as

$$z = b_0 + b_1 x + b_2 y \tag{24}$$

where b_0, b_1, and b_2 are the parameters of the one order trend surface that can be obtained by the least square method.

Let (x_i, y_i, z_i) $(i = 1, \ldots, n)$ be n given data where (x_i, y_i) are the coordinates of the ith given point and z_i is the value of the ith given point. According to the least square method, we use these data to fit a plane so that the square sum of the deviation of the data to the plane is the minimized.

Let

$$Q = \sum_{i=1}^{n} (z_i - \hat{z}_i)^2 = \sum_{i=1}^{n} (z_i - b_0 - b_1 x_i - b_2 y_i)^2 \tag{25}$$

where $\hat{z}_i = b_0 + b_1 x_i + b_2 y_i$ $(i = 1, 2, \ldots, n)$ is the trend value of the ith given point. To make Q value the least, based on the mathematical analysis principles, we make the partial derivative of Q to b_0, b_1 and b_2 and let them be equal to zero.

$$\begin{cases} \frac{\partial Q}{\partial b_0} = -2\sum_{i=1}^{n} (z_i - b_0 - b_1 x_i - b_2 y_i) = 0 \\ \frac{\partial Q}{\partial b_1} = -2\sum_{i=1}^{n} (z_i - b_0 - b_1 x_i - b_2 y_i) x_i = 0 \\ \frac{\partial Q}{\partial b_2} = -2\sum_{i=1}^{n} (z_i - b_0 - b_1 x_i - b_2 y_i) y_i = 0 \end{cases} \tag{26}$$

After rearrangement, the linear equations including b_0, b_1 and b_2 are obtained (written $\sum_{i=1}^{n}$ to $\sum$):

$$\begin{cases} b_0 n + b_1 \sum x_i + b_2 \sum y_i = \sum z_i \\ b_0 \sum x_i + b_1 \sum x_i^2 + b_2 \sum x_i y_i = \sum z_i x_i \\ b_0 \sum y_i + b_1 \sum x_i y_i + b_2 \sum y_i^2 = \sum z_i y_i \end{cases} \tag{27}$$

Eq. (27) can also be written as matrix forms:

$$\begin{pmatrix} n & \sum x_i & \sum y_i \\ \sum x_i & \sum x_i^2 & \sum x_i y_i \\ \sum y_i & \sum x_i y_i & \sum y_i^2 \end{pmatrix} \begin{pmatrix} b_0 \\ b_1 \\ b_2 \end{pmatrix} = \begin{pmatrix} \sum z_i \\ \sum z_i x_i \\ \sum z_i y_i \end{pmatrix} \tag{28}$$

From these equations, the parameters b_0, b_1 and b_2 can be obtained. Substitute n given data (x_i, y_i, z_i) $(i = 0, 1, \ldots, n)$ into the one order trend surface equation, n trend values can be found

$$\hat{z}_i = b_0 + b_1 x_i + b_2 y_i \quad (i = 1, 2, \ldots, n). \tag{29}$$

And then we can obtain the deviation values

$$e_i = z_i - \hat{z}_i, \quad (i = 1, 2, \ldots, n). \tag{30}$$

Fig. 9 shows the relationship among given values, trend values and deviation values with the regression line.

The deviation value reflects the local variation characteristic. The positive expresses that the values are higher than the average variation trend and the negative expresses that the values are lower than average variation trend.

The vertical scaling indicates the factor of the compression or amplification of the graph in the vertical direction when all the data are mapped into some small area. The data in the area in that the measured values are smaller should be smaller, vice versa. So, the space variation character of the data can be reflected factually by using the deviation value as the estimation of the vertical scaling.

When fractal interpolation is performed in the rectangle area, the data on the regular grids can be expressed as $\{x_n, y_m, z_{n,m}\}$ $(n = 0, 1, \ldots, N; m = 0, 1, \ldots, M)$. Similarly, trend value and deviation value can be expressed as $\hat{z}_{n,m}$ and $e_{n,m}$ respectively.

Let

$$e = \max_{0 \leqslant n \leqslant N; 0 \leqslant m \leqslant M} \{|e_{n,m}|\} \tag{31}$$

then vertical scaling

$$s_{n,m} = e_{n,m}/e, \quad (n \in \{1, 2, \ldots, N\}; m \in \{1, 2, \ldots, M\}) \tag{32}$$

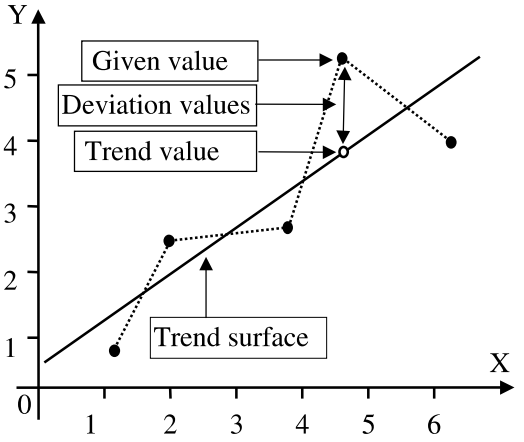

Fig. 9. The relationship among given values, trend values and deviation values.

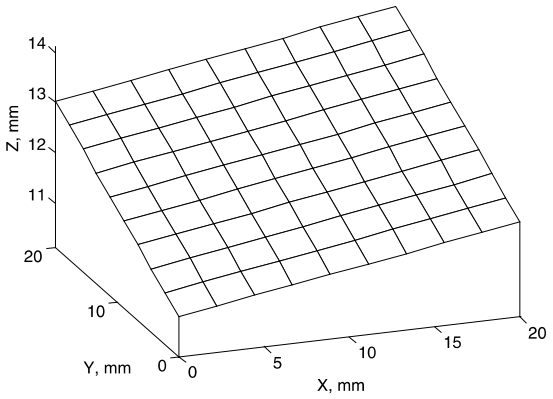

Fig. 10. One order trend surface.

4.3. Case study

In order to make comparisons conveniently, we also use the data in Table 1 as interpolating data. Using Eq. (24), we can get the one order trend surface (see Fig. 10). Using Eqs. (30)–(32), the vertical scaling can be obtained.

Combining with the partition of the local field discussed in the previous section, the local field is set in 4×4 points (see Fig. 8).

The fracture surface interpolated by using the improved self-affine fractal interpolation method is shown in Fig. 11.

Comparing Fig. 5 with Figs. 4 and 11, we can easily find that Fig. 11 can better express the real morphology of the fracture surface (Fig. 5). It is just because the method of improved self-affine fractal interpolation, the partition of local field and determination of vertical scaling, are used. Fig. 11 has higher precision than Fig. 4. We can say that the fracture surface generated by using the improved self-affine fractal interpolation method agrees well with the natural rock fracture surface.

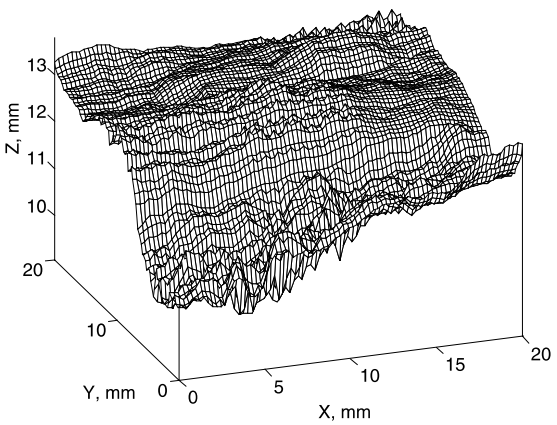

Fig. 11. Improved self-affine fractal interpolation surface.

It should be pointed out that sometimes the one order trend surface may include some interpolated points. That is to say, the observed value is equal to the trend value in some points. In this case the vertical scaling is zero. We can give the value less than 0.3 artificially. This work can be done easily by adding condition statements in the programming.

5. The relationship between the number of information points and the precision of the interpolation

The number of information points (the number of interpolating data) directly influences the interpolated result. In order to discuss the relationship between the amount of information points and the interpolation precision, the rock fracture surfaces of 12 samples are considered in this section. We select 6×6, 11×11, 21×21 and 41×41 data from the rock fracture surfaces to perform fractal interpolation and then compare the interpolated surfaces with the measured rock fracture surfaces. Finally, the power function of the relationship between the amount of information points and the interpolation precision is obtained.

5.1. Dimension precision

In engineering practice, the fractal dimension is an important parameter for fractal applications. In the research of roughness of rock fracture surfaces, it is also an essential index. For the interpolation theory of fractal surfaces, the fractal dimensions can be calculated from known information points and fractal interpolated surfaces. The problem is how to calculate the precision under the condition of certain known information points.

The information content is defined as the ratio of the amount of given information used in the fractal interpolation to the amount of total information. In the study of fractal interpolation surface, the information content is calculated as the percentage of the ratio of numbers of interpolating points used in fractal interpolating to the actual number of the data measured on rock fracture surfaces. That is

$$h = \frac{i_n}{f_n} \times 100\% \tag{33}$$

where i_n is the number of data used in fractal interpolation and f_n is the actual numbers of the data measured on rock fracture surfaces.

In engineering practice, the number of data used in fractal interpolation, i_n, is known and f_n is replaced by the total number of interpolated data in the fractal interpolation.

The dimension precision indicates the relationship of different information content used in the fractal interpolation and fractal dimension of the fractal interpolation surface. The dimension precision is then defined as

$$p_{\mathrm{d}} = 1 - \frac{|d_{\mathrm{i}} - d_{\mathrm{f}}|}{d_{\mathrm{f}}} \tag{34}$$

where d_{i} is the fractal dimension of fractal interpolation surface, d_{f} is the fractal dimension of the actual rock fracture surface.

Using the principle of the box covering method, the fractal dimension of the fractal interpolation surface and the actual rock fracture surface are calculated here approximately. For every sectional profile, we use five different lengths (scales) to perform net divisions. The minimum scale is equal to the minimum distance of every two data points, and the following scales are equal to twice that of the former. For every net, count up the number of meshes that intersect the surface. Calculate the logarithms of the scales and the corre-

sponding mesh numbers, and then use a straight line to fit these double-logarithm data. According to the slope of the straight line, we can obtain the fractal dimensions of sectional profiles. We take the average of these fractal dimensions plus one as the fractal dimension of the corresponding surface.

By Eq. (34), the dimension precision depends on the fractal dimension of the actual rock fracture surface, but the fractal dimension of rock fracture surface varies according to the resolution. In this paper we use the rock fracture surface data provided by Wang (Wang, 1994). Cutting rock bores of radius 4.18 cm into rock samples of height 5.0 cm, Wang made rock fracture surfaces by Brazilian tests and modified shear tests. Then the central area of 20×20 mm^2 of every rock fracture surface was scanned by a laser profilometer. The scan step length was 0.25 mm. Thus there are 81×81 test points in the area, and we can get $81 \times 81 = 6561$ data on every rock fracture surface. Therefore, the previous minimum scale used to calculate the fractal dimension is equal to 0.25 mm. On the basis of this calculating method of fractal dimension we study the dimension precision in this paper.

In the process of interpolation, we choose the deviations, $s_{n,m}$, of interpolation data as the vertical scaling, which sets up the relationship between the fractal dimension of interpolated surfaces and the interpolation data.

Table 3 shows the fractal dimensions of the fractal interpolation surfaces generated with different information content, i.e. different number of information points. The number of information points in the table represents the product of the points in the direction x and the points in the direction y. The content of the table is the fractal dimensions of the rock fracture surfaces of 12 samples having the different information contents.

From Table 3, it is clear that generally the fractal dimensions of interpolated surfaces are closer to that of the measured rock fracture surfaces as the number of the interpolation points increases. But the rock sample 5, the fractal dimension of the interpolated surface with (11×11) points is smaller than that with (6×6) points and at the rock sample 9, the fractal dimension of the interpolated surface with (6×6) points is closer to the fractal dimension of the measured rock fracture surface than the others.

Table 4 lists the fractal dimension precision of 12 rock samples with (6×6), (11×11), (21×21) and (41×41) points based on Eq. (34).

Using the power function to fit the average values in Table 3, we can obtain the relationship between information content and dimension precision (see Fig. 12)

$$y = 0.9993x^{0.004} \tag{35}$$

where y is the dimension precision, x is the information content used in the interpolation. The correlation coefficient of the fitting is 99.23%.

It is clear, from Eq. (35), that given the information content used in the interpolation, the dimension precision of the fractal interpolation surface can be estimated.

5.2. Deviation precision

The dimension precision shows the interpolation precision in macrocosm, while the deviation precision indicates the interpolation precision in the local data variation feature.

Let z_i $(i = 1, 2, \ldots, n)$ be n data measured on a rock fracture surface and $\hat{z}_i$ $(i = 1, 2, \ldots, n)$ be n fractal interpolated data. Then the average deviation is defined as

$$w = \frac{1}{n}\sum_{i=1}^{n}|z_i - \hat{z}_i| \tag{36}$$

From Eq. (36), the average deviation is the average value of the absolute error that contains the incorporation of the original data. If the average deviation of the first set of data is 1 with the average value of

Table 3
The dimension precision of fractal interpolation surface

Surface type	Number of data	Information content (%)	The rock sample code												Average
			1	2	3	4	5	6	7	8	9	10	11	12	
Fractal interpolation surface	6×6	0.55	0.9821	0.9890	0.9809	0.9797	0.9883	0.9754	0.9696	0.9818	0.9937	0.9565	0.9833	0.9771	0.9798
	11×11	1.84	0.9855	0.9891	0.9860	0.9894	0.9878	0.9799	0.9780	0.9844	0.9847	0.9687	0.9862	0.9836	0.9836
	21×21	6.72	0.9898	0.9957	0.9934	0.9929	0.9921	0.9866	0.9847	0.9907	0.9895	0.9812	0.9914	0.9890	0.9898
	41×41	25.62	0.9927	0.9969	0.9947	0.9965	0.9947	0.9904	0.9883	0.9932	0.9905	0.9843	0.9948	0.9924	0.9924
Fracture surface	81×81	100	1.0000	1.0000	1.0000	1.0000	1.0000	1.0000	1.0000	1.0000	1.0000	1.0000	1.0000	1.0000	1.0000

Table 4
Average deviation of fractal interpolation surfaces

Surface type	Number of points	Information content (%)	The rock sample code												Average
			1	2	3	4	5	6	7	8	9	10	11	12	
Fractal interpolation surfaces	6×6	0.55	0.1176	0.1160	0.1590	0.1469	0.1355	0.1796	0.2022	0.2350	0.1780	0.1928	0.1160	0.1613	0.1617
	11×11	1.84	0.0883	0.0788	0.1081	0.0827	0.0891	0.1360	0.1244	0.1480	0.0974	0.1489	0.0788	0.1055	0.1072
	21×21	6.72	0.0577	0.0483	0.0687	0.0536	0.0551	0.0883	0.0893	0.0978	0.0659	0.1005	0.0483	0.0678	0.0701
	41×41	25.62	0.0311	0.0252	0.0303	0.0257	0.0265	0.0428	0.0445	0.0475	0.0304	0.0510	0.0252	0.0303	0.0342

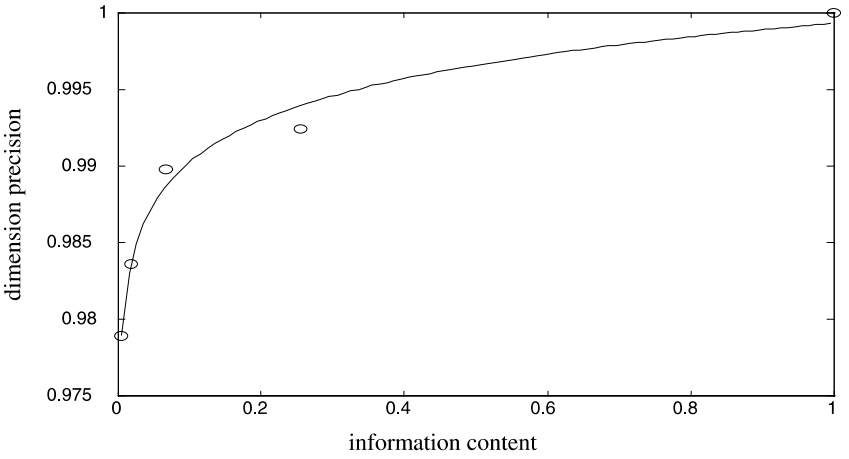

Fig. 12. The curve of dimension precision.

measured data 10 and if the average deviation of the second set of data is 1 too with the average value of measured data 5, then we know clearly that the interpolation precision of these two sets of data is different. The former is 90% and the latter 80%. The deviation precision is to express the interpolating precision by using deviation. In order to eliminate the influences of the original data, the deviation precision is obtained by dividing the average deviation by the average value of the original data. In fact, the greater the deviation is, the lesser the precision. To make the computing results agree with the definition of precision, the deviation precision is defined below:

$$p_z = 1 - \frac{w}{\frac{1}{n}\sum_{i=1}^{n} z_i} \tag{37}$$

The physical meaning of Eq. (37) can be regarded as: if the average deviation $w = 0$, the deviation precision $p_z = 1$; if the average deviation is equal to the average value of the original data, the deviation precision $p_z = 0$. When p_z is smaller than zero, that is to say, $w > (1/n)\sum_{i=1}^{n} z_i$, the average deviation is greater than the average value of the original data, then we say the estimation precision is zero. Therefore, the lesser the average deviation w is, the greater p_z is. The maximum of p_z is 1 and the minimum is 0. So p_z can be used as the precision and Eq. (37) is called deviation precision.

The amount of measured data on the rock fracture surface is 81×81. We select (6×6), (11×11), (21×21) and (41×41) data from each of the 12 rock fracture surfaces and interpolate them into 81×81 data, respectively. The average deviation of the interpolation is calculated by Eq. (37).

Table 5 gives the deviation of fractal interpolation surface of 12 rock fracture surfaces with information points (6×6), (11×11), (21×21) and (41×41).

From Table 5, it is seen that the average deviations of the 12 rock samples decrease with the increasing of the information content used in the interpolation. But it only gives us the absolute error and we do not know the precision. To eliminate the influences of the average data, we calculate the deviation according to Eq. (37) as shown in Table 6.

We can find the relationship of the information content and the deviation precision by fitting the average data in Table 6

$$y = 1.0034x^{0.0172} \tag{38}$$

where y is the deviation precision, x is the information content used in the interpolation. The correlation coefficient of the fitting is 99.26%.

Table 5
The deviation precision of the interpolation surfaces

Surface type	Number of points	Information contents (%)	The rock sample code												Average
			1	2	3	4	5	6	7	8	9	10	11	12	
Fractal interpolation surfaces	6×6	0.55	0.9006	0.9204	0.9272	0.9216	0.9236	0.9136	0.8837	0.9106	0.9403	0.8578	0.9204	0.9261	0.9122
	11×11	1.84	0.9254	0.9460	0.9505	0.9559	0.9498	0.9346	0.9284	0.9437	0.9674	0.8902	0.9460	0.9517	0.9408
	21×21	6.72	0.9513	0.9669	0.9685	0.9714	0.9689	0.9575	0.9486	0.9628	0.9779	0.9258	0.9669	0.9689	0.9613
	41×41	25.62	0.9737	0.9827	0.9861	0.9863	0.9851	0.9794	0.9744	0.9819	0.9898	0.9624	0.9827	0.9861	0.9809

Table 6
The relationship between the interpolation point number and the interpolation precision

Surface type	Point number	Information content (%)	Dimension precision	Deviation precision
Fractal interpolation surfaces	6×6	0.55	0.9798	0.9122
	11×11	1.84	0.9836	0.9408
	21×21	6.72	0.9898	0.9613
	41×41	25.62	0.9924	0.9809
Fracture surfaces	81×81	100	1.0000	1.0000

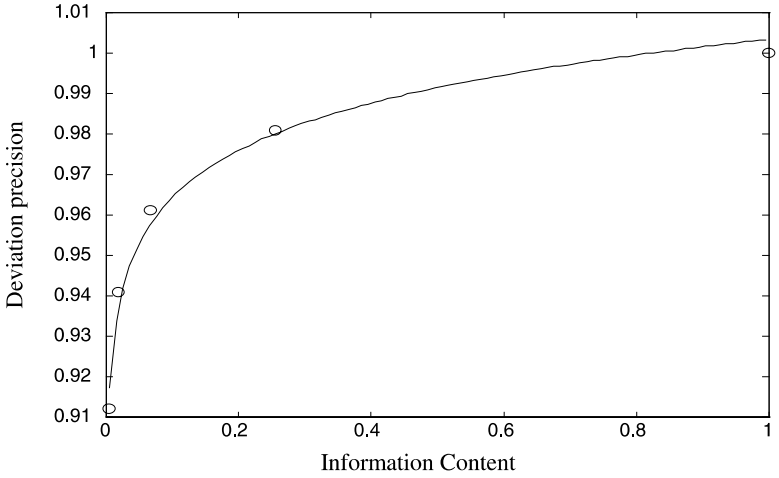

Fig. 13. The curve of deviation precision.

In engineering practice, if the percentage of the ratio of the number of data used in the interpolation to the total number of interpolated data is given, deviation precision of the fractal interpolation surface can be estimated from Eq. (38).

It should be pointed out, similar to the dimension precision, we actually do not know the total information amount in practical work. Then we use the total number of interpolated data as the total information amount.

For example, if we have 10 given interpolating data points and the total number of the interpolated data points is 100, the information content $x = 10/100 = 0.1$ and the deviation precision $y = 0.9644$. It means that the roughness of interpolated surface represents 96.44% of the actual fracture surface.

Fig. 13 shows the relationship of the information content and the interpolation deviation precision. From Fig. 13, we can see that this relationship is nonlinear. When the information content rises from 1/200 to 20/100, the interpolation deviation precision increases quickly. When the information amount rises from 20% to 100%, the interpolation deviation precision increases slowly. That is to say, in this scope the interpolation precision does not increase too much even if we increase many information points.

6. The fractal interpolation surfaces of rock feature surfaces

We have analyzed quantitatively the relationship between information amount used in interpolating and the interpolating precision. Fig. 14 shows the fractal interpolation surfaces of a rock fracture surface using the information data (6×6), (11×11), (21×21) and (41×41). The influence of the number of interpolating data to the interpolated surfaces can be objectively observed in Fig. 14. With the increase of the number of data points used in the interpolation, the morphologies of the fractal interpolation surfaces are closer to the ones of the measured rock fracture surfaces.

Fig. 15 gives two rock fracture surfaces of 12 rock samples and their corresponding fractal interpolation surfaces with the information content of 25.62% (i.e. 41×41 data).

Finally, according to the average index of 12 samples, the relationship between the interpolation point number and interpolation precision can be calculated and shown in Table 6.

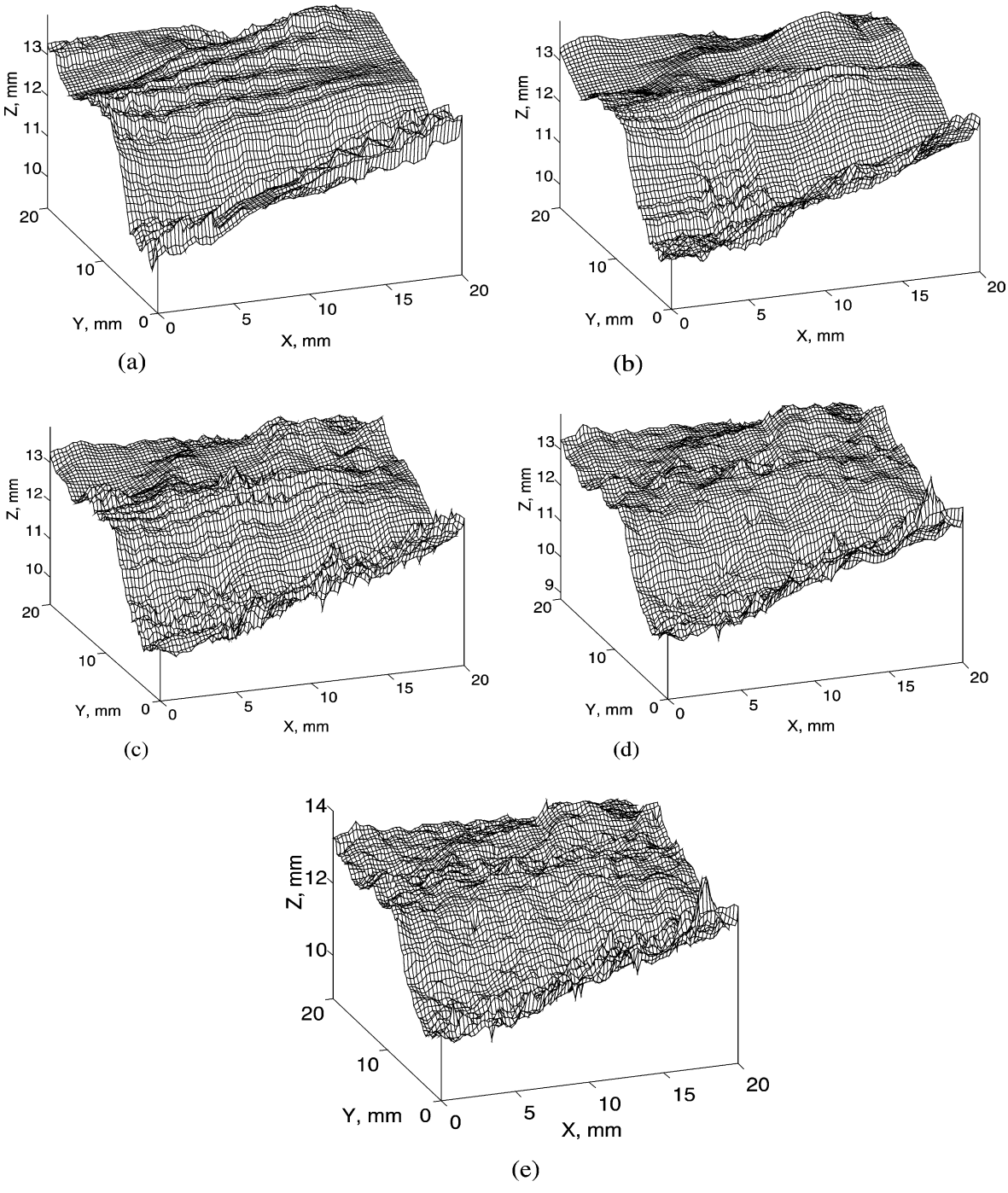

Fig. 14. Fractal interpolation surfaces with different information points: (a) information points 6×6, dimension = 2.0379; (b) information points 11×11, dimension = 2.0432; (c) information points 21×21, dimension = 2.0450; (d) information points 41×41, dimension = 2.0522; (e) measured rock fracture surface 81×81, dimension = 2.0589.

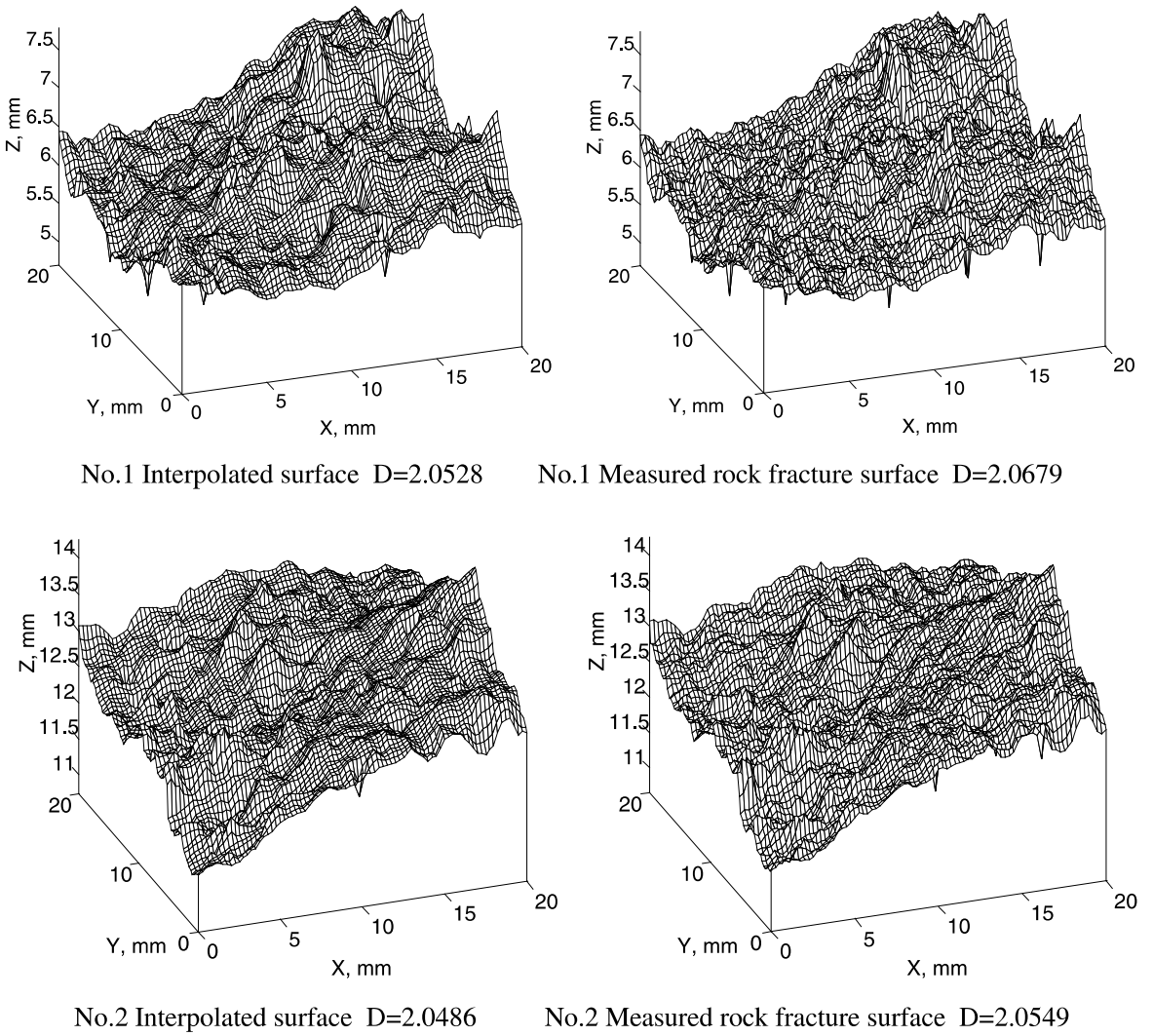

Fig. 15. Fractal interpolation surfaces and rock fracture surfaces of two rock samples (information content is 25.62%).

7. Conclusions

Usually, the fracture surface in rocks appears to be statistically self-similar and/or self-affine. The fractal geometry supplies an alternative method to describe quantitatively the roughness of fracture surfaces in rocks. Extensive studies show that the morphology of fracture surfaces in rocks really affects the degree of the accidents of slope instability and roof caving in civil and mining engineering. However, for a geological fault and joint in rocks, to obtain the morphology of whole fault surface is really difficult. It is to say that, in rock engineering, only a little information about roughness of a fault can be obtained from the exposure and several drill holes. The important work is how to estimate the morphology of fracture surfaces according to a little information from the surface. Therefore, the theory and method of fractal interpolation is needed to develop a new way to estimate the morphology of an entire fault surface from a little information of the morphology.

In this paper, an improved self-affine fractal interpolation method is proposed. The variagram in geostatistics is introduced into the fractal interpolation of rock fracture surfaces and the method of the local domain partition is established. By use of the principles of the trend surface analyses, the deviations on the information points are used as a vertical scaling factor.

Based on all of these improvements, some new concepts such as the precision of fractal dimension and deviation precision are put forward and a mathematical model of fractal interpolation surface is developed. Some case studies presented in this paper demonstrate that the method of fractal interpolation surface is very useful tool for simulation or generation of the morphology of rock fracture surfaces. It can be used to obtain very similar surfaces to a natural fracture surface using not more than a quarter of information points.

References

Aydan, Ö., Kawamoto, T., 1990. Discontinuities and their effects on rock mass. In: Barton, N., Stephansson, O. (Eds.), Rock Joints. Balkema, Rotterdam, pp. 149–156.

Bandis, S.C., 1990. Mechanical properties of rock joints. In: Barton, N., Stephansson, O. (Eds.), Rock Joints. Balkema, Rotterdam, pp. 125–140.

Barnsley, M.F., 1988. Fractals Everywhere. Academic Press, Orlando, FL, pp. 172–247.

Barnsley, M.F., Pemko, S.G., 1986. Iterated function systems and the global construction of fractals. Proc. Royal Soc. Lond. A 399, 243–275.

Barton, N., 1973. Review of a new shear strength criterion for rock joints. Engng Geol. 7, 287–322.

Byerlee, J.D., 1978. Friction of rocks. Pure Appl. Geophys. 116, 615–626.

Feder, J., 1988. Fractals. Plenum press, New York, pp. 212–228.

Huang, S.L., et al., 1992. Application of fractal characterization and modelling to rock joint profiles. Int. J. Rock Mech. Min. Sci. Geomech. Abstr. 29 (2), 89–98.

Lee, Y.H., et al., 1990. The fractal dimension as a measure of the roughness of rock discontinuity profile. Int. J. Rock Mech. Min. Sci. Geomech. Abstr. 127, 453–464.

Maerz, N.H., Franklin, J.A., 1990. Roughness scale effect and fractal dimension. In: Pinto da Cunha, A. (Ed.), Scale Effect in Rock Masses, Proceedings of the First International Workshop on Scale effects in Rock Masses. Balkema, Rotterdam, pp. 121–126.

Mandelbrot, B.B., 1982a. The Fractal Geometry of Nature. W.H. Freeman, New York, pp. 361–366.

Mandelbrot, B.B., 1982b. The Fractal Geometry of Nature. W.H. Freeman, New York, p. 468.

Massopust, P.R., 1994. Fractal Functions, Fractal Surface, and Wavelets. Academic Press, New York, pp.135–355.

Muralha, J., 1992. Fractal dimension of jointed roughness surface. Proceedings of ISRM Symposium Fractured and Jionted Rock Masses. Lake Taoe.

Odling, N.E., 1994. Natural fractal profiles, fractal dimension and joint roughness coefficients. Rock Mech. Rock Engng. 27 (3), 135–153.

Qi, D., 1994. Fractal and Its Computer Construction. Science Press, Beijing, pp. 70–72 (in Chinese).

Sun, H., 1990. Geostatistics and Its Applications. China University of Mining and Technology Press (in Chinese).

Turk, N., Grieg, M.J., Dearman, W.R., et al., 1987. Characterization of Rock Joint Surface by Fractal Dimension. In: Farmer, I.M. (Ed.), Rock Mechanics: Proceedings 28th US Symposium Rock Mechanics A.A. Balkema, Rotterdam, pp. 1223–1236.

Wang, X., 1982. Multivariable Statistical Analysis of Geological Data. Science Press (in Chinese).

Wang, J., 1994. Morphology and Mechanical Behavior of Rock Joints. Doctoral Thesis, Silesian Technical University, Gliwice, Poland.

Xie, H., 1989. Fractal effect of irregularity of crack branching on the fracture roughness of brittle materials. Int. J. Fract 40 (4), 267–274.

Xie, H., 1993. Fractals in Rock Mechanics. Balkema, Rotterdam, pp. 453.

Xie, H., Pariseau, W.G., 1994. Fractal estimation of joint roughness coefficients. Sci China Series B 37 (12), 1516–1524.

Xie, H., Sanderson, D.J., 1994. Fractal kinematics of crack propagation in geomaterials. Engng Fract Mech. 50 (4), 529–574.

Xie, H., Sanderson, D.J., 1995. Fractal effect of crack propagation on dynamic stress intensity and crack velocities. Int. J. Fract 74, 29–42.

Xie, H., Sun, H., 1997. The study on bivariate fractal interpolation functions and creation of fractal interpolated surfaces. Fractals 5 (4), 625–634.

Xie, H., et al., 1997. Fractal effects of surface roughness on the mechanical behavior of rock joints. Chaos Solids Fractals 8 (2), 221–252.

Xie, H., et al., 1998. The influence of proximate fault morphology on ground subsidence due to extraction. Int. J. Rock Mech. Min. Sci. Geomech. Abstr. 35 (8), 1107–1111.